

Unmasking of CD22 Co-receptor on Germinal Center B-cells Occurs by Alternative Mechanisms in Mouse and Man*

Received for publication, September 10, 2015, and in revised form, October 14, 2015. Published, JBC Papers in Press, October 27, 2015, DOI 10.1074/jbc.M115.691337

Matthew S. Macauley[‡], Norihito Kawasaki^{†1}, Wenjie Peng[§], Shui-Hua Wang[¶], Yuan He[§], Britni M. Arlian[§], Ryan McBride[§], Reiji Kannagi^{||}, Kay-Hooi Khoo[¶], and James C. Paulson^{‡§***2}

From the Departments of [‡]Chemical Physiology, [§]Cell and Molecular Biology, and ^{**}Immunology and Microbial Science, The Scripps Research Institute, La Jolla, California 92037 and the Institutes of [¶]Biological Chemistry and ^{||}Biomedical Science, Academia Sinica, Taipei 115, Taiwan

Background: Changes in glycosylation on germinal center B-cells have the potential to influence CD22.

Results: CD22 is unmasked on germinal centers due to loss of its preferred ligand.

Conclusion: Different biosynthetic mechanisms in mice and humans down-regulate the preferred CD22 ligand on germinal center B-cells.

Significance: Conserved unmasking of CD22 on germinal center B-cells from mice and humans suggests an important role for CD22 in the germinal center.

CD22 is an inhibitory B-cell co-receptor whose function is modulated by sialic acid (Sia)-bearing glycan ligands. Glycan remodeling in the germinal center (GC) alters CD22 ligands, with as yet no ascribed biological consequence. Here, we show in both mice and humans that loss of high affinity ligands on GC B-cells unmasks the binding site of CD22 relative to naive and memory B-cells, promoting recognition of *trans* ligands. The conserved modulation of CD22 ligands on GC B-cells is striking because high affinity glycan ligands of CD22 are species-specific. In both species, the high affinity ligand is based on the sequence Sia α 2–6Gal β 1–4GlcNAc, which terminates *N*-glycans. The human ligand has *N*-acetylneuraminic acid (Neu5Ac) as the sialic acid, and the high affinity ligand on naive B-cells contains 6-*O*-sulfate on the GlcNAc. On human GC B-cells, this sulfate modification is lost, giving rise to lower affinity CD22 ligands. Ligands of CD22 on naive murine B-cells do not contain the 6-*O*-sulfate modification. Instead, the high affinity ligand for mouse CD22 has *N*-glycolylneuraminic acid (Neu5Gc) as the sialic acid, which is replaced on GC B-cells with Neu5Ac. Human naive and memory B-cells express sulfated glycans as high affinity CD22 ligands, which are lost on GC B-cells. In mice, Neu5Gc-containing glycans serve as high affinity CD22 ligands that are replaced by Neu5Ac-containing glycans on GC B-cells. Our results demonstrate that loss of high affinity CD22 ligands on GC B-cells occurs in both mice and humans through alternative mechanisms, unmasking CD22 relative to naive and memory B-cells.

CD22 is an inhibitory co-receptor of the B-cell receptor (BCR)³ and a member of the sialic acid-binding immunoglobulin-type lectin (siglec) family, which recognize Sia-containing glycans on glycoproteins and glycolipids (1). CD22 can engage its glycan ligands on the same cell (*cis*) or an opposing cell (*trans*), both of which have the ability to regulate the function of CD22 through modulating its association with the BCR (1, 2). Studies ablating CD22-ligand interactions have concluded that *cis* ligands limit CD22 association with the BCR (3, 4), and less dramatic alterations to *cis* ligands can provide a finer control over CD22-BCR association (5, 6). In contrast, *trans* ligands on a contacting cell displaying an antigen recognized by the BCR draw CD22 into the immunological synapse to inhibit B-cell activation (7, 8). In addition to regulating the association of CD22 with the BCR, *trans* CD22-ligand interactions are also involved in B-cell homing (9, 10). Although *cis* ligands “mask” the ability of CD22 to interact with *trans* ligands (11), through setting a threshold for *trans* ligand engagement, *cis* ligands do not prevent binding to *trans* ligands (12, 13). Thus, the interplay of *cis* and *trans* CD22-ligand interactions has the ability to affect the function of CD22 on naive follicular B-cells in many ways. Much less is known, however, about the role of CD22-ligand interactions on subsequent stages of B-cell differentiation, such as germinal center (GC) and memory B-cells.

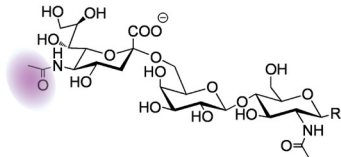
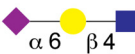
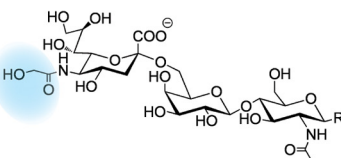
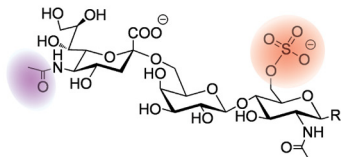
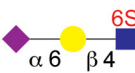
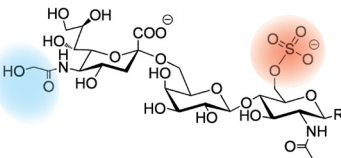
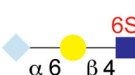
The GC is a spatially and temporally regulated anatomic location where antibody affinity maturation takes place (14). Glycan remodeling in the GC has been known to occur for some time, through staining of the GC by the lectin peanut agglutinin and the carbohydrate-recognizing antibody GL7. Furthermore, in both mice and humans immunohistochemical staining has revealed that the GC fails to stain with recombinant CD22-Fc

* This work was supported by National Institutes of Health Grants AI099141 and AI050143 (to J. C. P.). The authors declare that they have no conflicts of interest with the contents of this article. The content is solely the responsibility of the authors and does not necessarily represent the official views of the National Institutes of Health.

¹ Present address: Food and Health Institute Strategic Program, Institute of Food Research, Norwich, Norfolk NR47UA, United Kingdom.

² To whom correspondence should be addressed: Dept. of Cell and Molecular Biology, The Scripps Research Institute, 10550 North Torrey Pines Rd., MB-202, La Jolla, CA 92037. Tel.: 858-784-9634; Fax: 858-784-9690; E-mail: jcpaulson@scripps.edu.

³ The abbreviations used are: BCR, B-cell receptor; GC, germinal center; Neu5Ac, *N*-acetylneuraminic acid; Neu5Gc, *N*-glycolylneuraminic acid; PEG, polyethylene glycol; HBSS, Hanks' balanced saline solution; LEL, *Lycopersicon esculentum* lectin; LacNAc, Gal β 1–4GlcNAc; DSPE, distearoyl phosphoethanolamine; CFSE, carboxyfluorescein diacetate succinimidyl ester; SNA, *S. nigra* lectin; h, human; m, mouse; PE, phycoerythrin; Sia, sialic acid.

Chemical Structure and Name	Symbol Structure	Antibody Specificity	
		GL7	KN343
 <p>Neu5Acα2-6Galβ1-4GlcNAc</p>	 <p>α 6 β 4</p>	+	-**
 <p>Neu5Gcα2-6Galβ1-4GlcNAc</p>	 <p>α 6 β 4</p>	-*	-**
 <p>Neu5Acα2-6Galβ1-4(6S)GlcNAc</p>	 <p>α 6 β 4 6S</p>	+	+***
 <p>Neu5Gcα2-6Galβ1-4(6S)GlcNAc</p>	 <p>α 6 β 4 6S</p>	-***	+***

 <i>N</i> -glycoylneuraminic acid (Neu5Gc)	 Galactose (Gal)
 <i>N</i> -acetylneuraminic acid (Neu5Ac)	 <i>N</i> -acetylglucosamine (GlcNAc)
	 6-sulfo- <i>N</i> -acetylglucosamine (6S-GlcNAc)

FIGURE 1. Glycan structures relevant to CD22 ligands on murine and human B-cells. The following trisaccharides on complex *N*- and *O*-glycans serve as potential CD22 ligands. These four structures differ in the form of sialic acid or *N*-acetylglucosamine modification. The sialic acid can be Neu5Gc (light blue diamond) or Neu5Ac (purple diamond) α 2-6-linked to an underlying Gal (yellow circle), which is itself linked to a GlcNAc (blue square) via a β 1-4 linkage. The GlcNAc residue has the possibility of being sulfated at that 6-position (red highlight). This trisaccharide can terminate complex *N*- and *O*-glycans (underlying glycan designated by *R*). These structural features are differentially expressed on different B-cell subsets in mice and humans, as detected by the antibodies GL7 and KN343 in mice and humans, respectively. *, established previously (6); **, established previously (15); ***, determined in work described in this study.

compared with bright staining of the outer mantle zone where naive follicular B-cells are located (6, 15). This staining pattern indicates that there are lower levels of CD22 ligands in the GC. Given the important roles played by CD22-ligand interactions, alterations in CD22 ligands in the GC strongly suggest a biological function.

The nature of changes in glycosylation that reduce levels of CD22 ligands in the GC has been investigated in several pioneering studies (6, 15). In mice, loss of CD22 ligands on GC B-cells was attributed to the down-regulated expression of *CMP-N*-acetylneuraminidase monooxygenase (6), which is the sole enzyme that creates the cellular source of *N*-glycoylneuraminic acid (Neu5Gc) (16). As a consequence, there is an appearance of *N*-acetylneuraminic acid (Neu5Ac) on GC B-cells, which is revealed by staining with the antibody GL7 (6). This change impacts the *cis* ligands of murine CD22, which exhibits >10-fold high affinity for Neu5Gc α 2-6 linked to an underlying LacNAc (Gal β 1-4GlcNAc), compared with the

corresponding sialoside containing Neu5Ac (Fig. 1) (17, 18). Therefore, loss of *CMP-N*-acetylneuraminidase monooxygenase expression is responsible for loss of CD22 ligands on GC B-cells, which is mediated through loss of Neu5Gc.

Humans have lost the ability to produce Neu5Gc due to inactivation of the gene encoding *CMP-N*-acetylneuraminidase monooxygenase (16). However, an alternative mechanism has been proposed to account for loss of high affinity ligands of CD22 in the GC in humans (15). Human CD22 recognizes the structure Neu5Ac α 2-6Gal β 1-4(6-sulfo)GlcNAc (Fig. 1) as a high affinity ligand (17), and an antibody that recognizes this structure, KN343, was shown to stain the mantle zone but not the GC in human tonsils (15). Several pieces of evidence suggest that the sulfotransferase responsible for creating the KN343 epitope on human lymphocytes is HEC-GlcNAc6ST (15, 19). These results suggest that loss of this sulfate modification on human GC B-cells may give rise to a loss of high affinity ligands. Confirmation that human GC B-cells have low levels of CD22

Unmasking of CD22 in the Germinal Center

ligands has not been presented nor has this sulfate modification been directly observed on human B-cells.

Here, we show that changes in CD22 ligands on GC B-cells have significant functional consequences in CD22 recognition of *trans* ligands. Specifically, we show in both mice and humans that CD22 is unmasked on GC B-cells relative to their naive B-cell counterparts, and this effect is transient because the glycans on memory B-cells return to conditions observed on naive follicular B-cells, returning CD22 to a fully masked state. Mass spectrometry glycomic profiling of human B-cells, biochemical characterization of GL7 and KN343 antibody specificities by glycan microarrays, and analysis of CD22 binding affinity with synthetically prepared sialosides cumulatively provide strong evidence that unmasking of CD22 on GC B-cells occurs in both mice and humans, yet through different mechanisms that are tailored to the glycans found on murine and human B-cells.

Experimental Procedures

Materials—Magnetic beads (6.7×10^8 beads/ml; Life Technologies, Inc., M-280 Dynabeads, catalog no. 112.06D), glycan polymer Neu5Gc α 2–6Gal β 1–4GlcNAc-polyacrylamide-biotin (PA365, 1 MDa; Consortium for Functional Glycomics Reagent Bank), HBSS/BSA buffer (Hanks'-buffered saline solution, 0.5% bovine serum albumin), anti-human IgG-FITC (Jackson ImmunoResearch), and 6-O-sulfate-LacNAc (from Nicolai V. Bovin Laboratory, Institute of Bioorganic Chemistry, Russian Academy of Sciences) were obtained.

Mice—C57BL/6J mice were maintained in a specific pathogen-free condition in the animal facility at The Scripps Research Institute and used in the accordance with the guidelines of the Institutional Animal Care and Use Committee.

Cloning and Expression of Human and Murine CD22-hIgG1-Fc Chimeras—Human IgG1-Fc was subcloned from the pFuse-hIgG1-Fc vector into the pcDNA5/FRT/V5-His-TOPO vector into the AgeI restriction site, such that the 3' site was destroyed by ligation of AgeI and Aval cut sites. A stop coding was not included, such that the protein would encode a C-terminal His₆ tag for purification purposes. Amino acid residues 1–332 of human CD22 or residues 1–353 of murine CD22 were subsequently cloned into this vector using the NheI and AgeI restriction sites. Flp-In CHO cells were transfected with plasmid encoding either human CD22-Fc or murine CD22-Fc, and cells were selected in media (DMEM/F-12, 10% FCS, penicillin/streptomycin) containing 0.75 mg/ml hygromycin for 12 days, after which cells were maintained in 0.5 mg/ml hygromycin. For production, cells were grown to near confluence in a T-175 flask and transferred to a 2-liter roller bottle containing 500 ml of media. Bottles were rotated at a speed of 0.5 rpm at 37 °C for 12 days. The supernatant was centrifuged (270 relative centrifugal force; 7 min) to remove cell debris and filtered through a 200-micron filter. Clarified supernatants were concentrated 5-fold using a tangential flow filtration cartridge system (Millipore), supplemented with 5 mM imidazole, and loaded at 4 ml/min onto a HisTrap HP 5-ml column (GE Healthcare) pre-equilibrated with 50 ml of binding buffer (500 mM NaCl, 20 mM Na₂HPO₄, 5 mM imidazole, pH 7.6). The column was washed with 100 ml of binding buffer + 60 mM imidazole and eluted with 25 ml of binding buffer + 250 mM imidazole. Protein yield

was 8–10 mg/500 ml and was highly pure as judged by SDS-PAGE.

Cells—Human peripheral blood and tonsils were obtained from healthy human donors and patients undergoing tonsillectomy, respectively, according to the Institutional Review Board at The Scripps Research Institute. In both cases, human lymphocytes were isolated by a density-gradient centrifugation using Ficoll Plus (GE Healthcare). If needed, B-cells were further purified with a negative selection using B-cell isolation kit II (Miltenyi Biotec).

Immunization of Mice—Mice were immunized via an intraperitoneal injection of 200 μ g of ovalbumin emulsified in Alum. Three weeks later, mice were boosted in the same way, and spleens were analyzed 10 days later.

Antibodies—Antibodies used for flow cytometry included those against human CD3 (UCHT1, BD Biosciences), CD19 (HIB19, BioLegend), CD22 (HIB22, BioLegend), CD27 (O323, BioLegend), CD38 (HIT2, BioLegend), and mouse CD5 (53–7.3, BioLegend), CD19 (6D5, BioLegend), CD22 (OX-97, BioLegend), CD38 (90, BioLegend), CD73 (TY/11.8, BioLegend), CD80 (16–10A1, BioLegend), and IgD (11–26c.2a, BioLegend). Anti-glycan antibodies included GL-7 (GL-7, BioLegend) and KN343 (15). All the isotype control antibodies used in this study were purchased from BioLegend.

Liposomes—Fluorescent liposomes were prepared as described previously (8). Briefly, all liposomes were composed of distearoyl phosphatidylcholine (Avanti Polar Lipids), cholesterol (Sigma), polyethyleneglycol-distearoyl phosphoethanolamine (PEG-DSPE, NOF America), and pegylated lipids in a 60:35:5 molar ratio. Naked liposomes contained 4.8 mol % PEG-DSPE and 0.2 mol % Alexa 647-PEG-DSPE. Human and mouse CD22-specific liposomes substituted 1 mol % ^{MPB}Neu5Aca2–6Gal β 1–4GlcNAc-lipid or 1 mol % ^{BPA}Neu5Gca2–6Gal β 1–4GlcNAc-lipid with equivalent amounts of PEG-DSPE, respectively. For liposome preparation, lipid components in dimethyl sulfoxide (CD22 ligand/lipid and Alexa 647-PEG-DSPE) were mixed and lyophilized in a glass tube. The other components in chloroform were then added to the tube and dried completely by evaporation with nitrogen. The dried lipids were hydrated with 1 ml of PBS, sonicated, and extruded through an extruder (Avanti Polar Lipids) to a diameter of 100 nm, as measured by a Zetasizer (Malvern).

Flow Cytometry—Cells were suspended in HBSS containing 0.1% BSA, 2 mM EDTA, and 0.1% NaN₃ (FACS buffer), blocked with anti-human CD32 (3D3, BD Biosciences) or anti-mouse Fc blocking antibody (93, BioLegend) for 5 min at 25 °C, and stained with fluorescently labeled antibodies for 30 min at 4 °C. Stained cells were washed once with FACS buffer using a FACSCalibur or LSR II flow cytometer (BD Biosciences). Propidium iodide (1 mg/ml) was added to the sample before the analysis for exclusion of the dead cells. Acquired data were analyzed with Flowjo (Tree Star). For KN343 staining, cells were incubated with KN343 or mouse IgM (isotype control), followed by the staining with PE-labeled anti-mouse IgM^a (BioLegend). For the liposome binding analysis, cells were incubated with the liposomes for 30 min at 37 °C, then washed, and stained with the cell surface markers. FITC-labeled LEL (Vector Laboratories) was used at 1 μ g/ml.

In Vitro B-cell Activation—Purified B-cells were suspended at 1.0×10^7 cells/ml in HBSS containing 3% heat-inactivated FCS and 5 mM carboxyfluorescein diacetate succinimidyl ester (CFSE, Life Technologies, Inc.) for 7 min at 25 °C. CFSE-labeled B-cells were added in a 96-well plate at 2.0×10^5 cells/well in the 200 μ l of RPMI 1640 medium (Life Technologies, Inc.) supplemented with 10% heat-inactivated FCS, 2 mM glutamine, 100 units/ml penicillin, 100 μ g/ml streptomycin, 1 mM non-essential amino acids, 1 mM sodium pyruvate, 50 μ M 2-mercaptoethanol, 10 μ g/ml F(ab')₂ anti-human IgA, IgG, and IgM (Jackson ImmunoResearch), and 50 nM CpG2006 (Invivogen). At day 3, cells were then harvested, stained with KN343, and analyzed by flow cytometry.

ELISA for GL7 Specificity—ELISA plates were coated overnight with 5 μ g/ml GL7 (BioLegend). The following day, the plate was blocked in 0.1% BSA in PBS for 30 min at room temperature prior to incubation with the glycans for 2 h at room temperature with 2-fold serial dilutions starting at 400 μ M. Plates were washed four times with PBS and incubated for 1 h at room temperature with avidin-HRP. Following five washes, plates were developed with tetramethylbenzidine substrate for 15 min at room temperature and quenched with 2 M sulfuric acid. Plates were read at 450 and 650 nm as a reference.

MS Analysis—Purified B-cells were washed three times with PBS. Washed cells were suspended in 100 mM ammonium bicarbonate, boiled for 10 min, and then lyophilized. Glycoproteins were extracted from the cell lysates using 6 M guanidine HCl, sequentially digested by trypsin and chymotrypsin after reduction/alkylation and dialysis, followed by release of *N*-glycans and *O*-glycans by peptide:*N*-glycosidase F digestion and reductive elimination in 1 M NaBH₄, 0.05 M NaOH, respectively, with and without additional digestion by α 2-3-sialidase (sialidase S, recombinant, *Escherichia coli*, Prozyme), as described in detail previously (20). Released glycans were permethylated, and permethylated sulfated glycans were enriched by amine beads for negative ion mode MALDI-TOF/TOF analysis on a 4700 Proteomic Analyzer, according to previously published protocols and MALDI-MS instrument settings (21).

Glycan Microarray—The ligand specificities of KN343, GL7, human CD22-Fc, murine CD22-Fc, and SNA were interrogated using a sialoside array. The sialoside array contains 59 compounds, one more than previously reported (22). KN343 antibody was tested at 10 μ g/ml for 1 h at 25 °C. The array was washed with PBS and probed with PE-labeled anti-mouse IgM for 1 h at 25 °C (5 μ g/ml, Jackson ImmunoResearch). For analysis of GL7 and SNA binding, directly conjugated GL7-FITC (BioLegend) and SNA-FITC (Vector Laboratories) were used at a concentration of 10 and 1 μ g/ml, respectively. Both murine CD22-Fc and human CD22-Fc were pre-complexed at a concentration of 10 μ g/ml with 5 μ g/ml PE-labeled anti-human IgG1 (Jackson ImmunoResearch). The signal was detected and measured using an Innoscan 1100AL confocal microarray scanner and Mapix software (Innopsys). Mean signal intensities of four spots were averaged.

Bead Binding Assay—Streptavidin-coated magnetic beads (20 μ l, 1.34×10^7 beads) were washed with HBSS/BSA and mixed with Neu5Gc α 2-6Gal β 1-4GlcNAc-polyacrylamide-biotin probe (1 mg/ml; 2 μ l) in HBSS/BSA buffer (200 μ l) for 2 h

at room temperature. Beads were washed with HBSS/BSA buffer (three times, 200 μ l) then resuspended in 200 μ l of HBSS/BSA buffer (6.7×10^7 beads/ml). The concentration of sialoside inhibitors was determined using the periodate-resorcinol assay. For the inhibition assay, serial dilutions of the sialoside inhibitors (50 μ l) were first added to the 96-well compatible flow cytometry tubes. Glycan polymer-coated beads (0.5 μ l) and anti-human/murine IgG-FITC (0.31 μ l) in 20 μ l of HBSS/BSA buffer were added, followed by addition of purified human/murine CD22-Fc (0.025 μ g in 30 μ l of HBSS/BSA buffer). After shaking for 30 min at room temperature, samples were analyzed by flow cytometry. All assays were carried out in triplicate, and three independent measurements were performed.

Oligosaccharide Synthesis—Neu5Ac α 2-6Gal β 1-4-GlcNAc β -ethyl azide and Neu5Gc α 2-6Gal β 1-4-GlcNAc β -ethyl azide were prepared as described previously (23). The biotinylated *N*-glycans were synthesized using a protocol that will be published elsewhere.

For Neu5Ac α 2-6Gal β 1-4(6-sulfo)GlcNAc β -ethylamine, 6-*O*-sulfate-LacNAc (2.0 mg, 3.95 μ mol), ManNAc (1.2 mg, 1.4 eq), sodium pyruvate (3.2 mg), CTP (2.9 mg), and aldolase (0.1 mg) were dissolved in 400 μ l of Tris-HCl buffer (50 mM, pH 8.5, with 15 mM MgCl₂). *Neisseria meningitidis* sialic acid synthetase (NmCSS) (50 milliunits) and hST6Gal-I (33 milliunits) were added to the mixture and incubated overnight at 37 °C. The reaction was monitored by TLC (iPrOH/NH₄OH/H₂O = 5:2:1) and stained with 10% sulfuric acid/ethanol solution. The insoluble precipitates were removed by centrifugation, and the supernatant was concentrated and purified by BioGel P-2 gel filtration column. Fractions were lyophilized to give the final product as a white powder (2.9 mg, 94% yield). ¹H NMR (600 MHz, D₂O), δ = 4.61 (d, *J* = 8.4 Hz, 1H), 4.46 (d, *J* = 8.0 Hz, 1H), 4.44 (dd, *J* = 11.2, 2.1 Hz, 1H), 4.30 (dd, *J* = 11.2, 5.5 Hz, 1H), 4.05–3.93 (m, 3H), 3.93–3.73 (m, 8H), 3.73–3.60 (m, 5H), 3.57–3.48 (m, 3H), 3.28–3.13 (m, 2H), 2.65 (dd, *J* = 12.4, 4.7 Hz, 1H), 2.06 (s, 3H), 2.01 (s, 3H), 1.71 (t, *J* = 12.2 Hz, 1H); ESI-MS *m/z* calculated for C₂₇H₄₈N₃O₂₂S [M + H⁺] was 798 and found was 798.

For Neu5Gc α 2-6Gal β 1-4(6-sulfo)GlcNAc β -ethylamine, 6-*O*-sulfate-LacNAc (2.0 mg, 3.95 μ mol), *N*-glycolylmannosamine (1.2 mg, 1.4 eq), sodium pyruvate (3.2 mg), CTP (2.9 mg), and aldolase (0.1 mg) were dissolved in 400 μ l of Tris-HCl buffer (50 mM, pH 8.5, with 15 mM MgCl₂). NmCSS (50 milliunits) and hST6Gal-I (33 milliunits) were added to the mixture and incubated overnight at 37 °C. The reaction was monitored by TLC (iPrOH/NH₄OH/H₂O = 5:2:1) and stained with 10% sulfuric acid/ethanol solution. The insoluble precipitates were removed by centrifugation, and the supernatant was concentrated and purified by BioGel P-2 gel filtration column. Fractions were lyophilized to give the final product as a white powder (2.9 mg, 94% yield). ¹H NMR (600 MHz, D₂O): δ = 4.66 (d, *J* = 8.1 Hz, 1H), 4.54–4.44 (m, 2H), 4.33 (dd, *J* = 11.2, 5.5 Hz, 1H), 4.14 (s, 2H), 4.09–3.63 (m, 16H), 3.62–3.53 (m, 3H), 3.35–3.16 (m, 2H), 2.71 (dd, *J* = 12.4, 4.7 Hz, 1H), 2.10 (s, 3H), 1.75 (t, *J* = 12.2 Hz, 1H); ESI-MS *m/z* calculated for C₂₇H₄₈N₃O₂₃S [M + H⁺] was 814 and found was 814.

Unmasking of CD22 in the Germinal Center

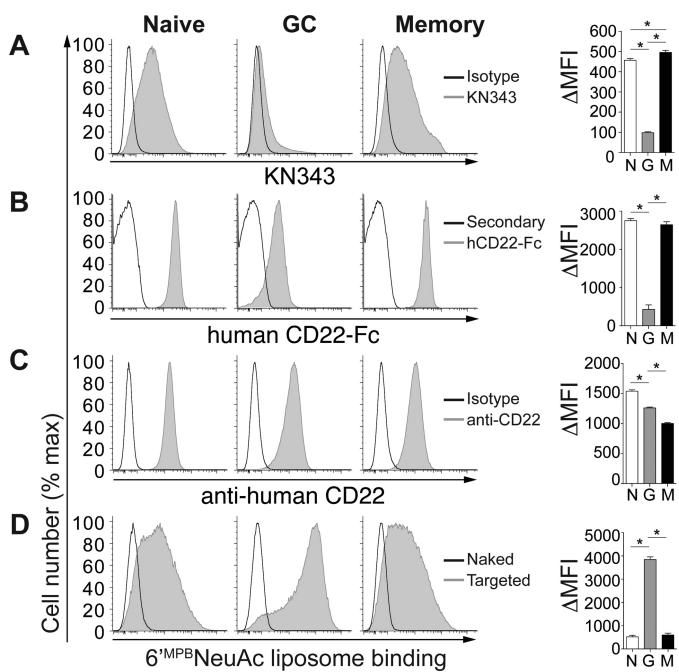


FIGURE 2. CD22 is unmasked on human GC B-cells compared with naive and memory B-cells. Flow cytometry staining of naive ($CD27^{-}CD38^{low}$), GC ($CD27^{+}CD38^{+}$), and memory ($CD27^{-}CD38^{-}$) human tonsillar $CD19^{+}$ B-cells with KN343 (A), human CD22-Fc (B), anti-human CD22 (C), and fluorescent liposomes (D) displaying no ligand (naked) or a selective human CD22 ligand ($6^{MPB}Neu5Ac$; targeted). Quantitated ΔMFI (mean fluorescence intensity) values represent background-subtracted values and represent the average and standard error of three replicates and is representative of three independent experiments. *, $p < 0.05$; N, naive; G, germinal center; M, memory. Statistical analysis was performed by Student's *t* test.

Statistical Analysis—Student's *t* test was used for statistical analysis using Prism software (GraphPad). $p < 0.05$ was considered as statistically significant.

Results

CD22 Is Unmasked on GC B-cells from Mouse and Human—To investigate how altered CD22 ligands on GC B-cells affect the ability of CD22 to recognize *trans* ligands, we carried out binding studies with fluorescent liposomal nanoparticles bearing selective ligands for human CD22 ($6^{MPB}Neu5Ac$) (24) and mouse CD22 ($6^{BPA}Neu5Gc$) (25). B-cells ($CD19^{+}CD3^{-}$) from human tonsils were analyzed by flow cytometry using markers for differentiating naive ($CD38^{low}CD27^{-}$), memory ($CD38^{-}CD27^{+}$), and GC ($CD38^{+}CD27^{+}$) B-cell populations (Fig. 2). GC B-cells stained low with KN343 compared with naive B-cells, whereas KN343 stained memory B-cells even slightly higher than naive B-cells (Fig. 2A). Minimal variation in staining with the $\alpha 2$ -6-specific *Sambucus nigra* (SNA) lectin was observed among subsets, indicating that the differential staining with KN343 is not due to loss of $\alpha 2$ -6-linked sialosides. GC B-cells stained low with human CD22-Fc, and there was no statistical difference between naive and memory B-cells (Fig. 2B). Cell surface levels of CD22 remained high on all three populations, although small differences were observed (Fig. 2C). Despite a similar amount of CD22, GC B-cells showed a clear advantage over naive and memory B-cells in their ability to recognize fluorescent liposomal nanoparticles bearing the human CD22 ligand $6^{MPB}Neu5Ac$ (Fig. 2D). This enhanced abil-

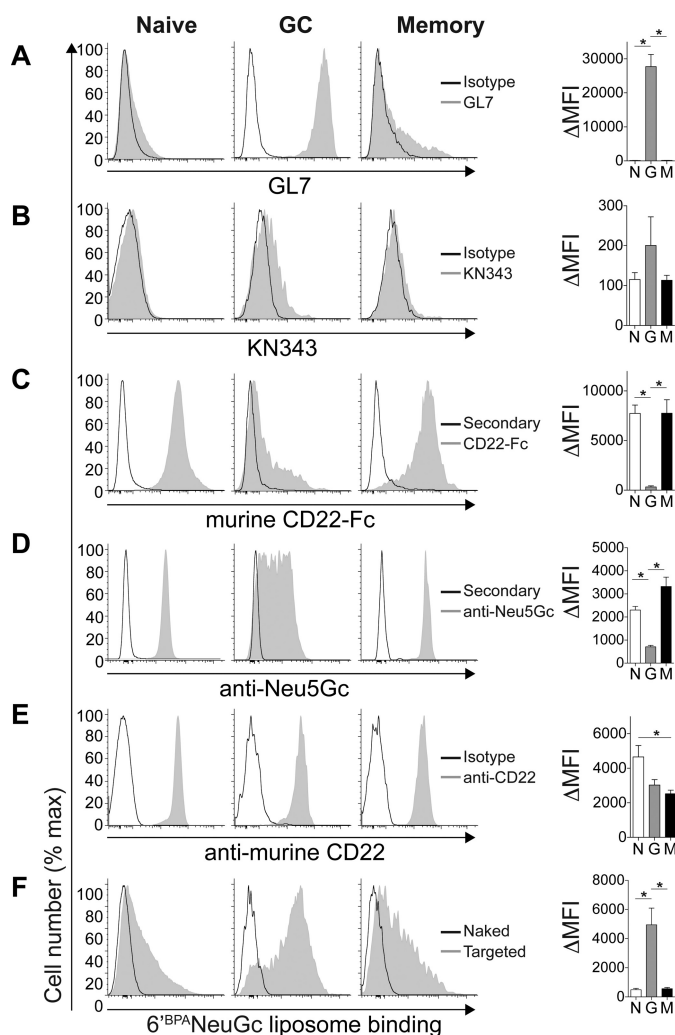


FIGURE 3. Unmasking of CD22 on murine GC B-cells relative to naive and memory B-cells. Flow cytometry staining of naive ($IgD^{+}CD38^{+}CD95^{-}$), GC ($CD38^{-}CD95^{+}$), and memory ($IgD^{-}CD38^{+}CD73^{+}CD80^{+}$) murine $CD19^{+}$ B-cells with GL7 (A), KN343 (B), murine CD22-Fc (C), anti-Neu5Gc (D), anti-murine CD22 (E), and fluorescent liposomes (F) displaying no ligand (naked) or a selective murine CD22 ligand ($6^{BPA}Neu5Gc$; targeted). Quantitated ΔMFI (mean fluorescence intensity) values represent background-subtracted values and represent the average and standard error of three replicates and is representative of three independent experiments. *, $p < 0.05$; N, naive; G, germinal center; M, memory.

ity of CD22 to recognize *trans* ligands demonstrates that CD22 is unmasked on human GC B-cells relative to naive and memory B-cells, which correlates with lower levels of CD22 ligands on these cells.

A parallel analysis was performed on mouse B-cells ($CD19^{+}$) for naive ($IgD^{+}CD38^{+}CD95^{-}$), GC ($CD38^{-}CD95^{+}$), and memory ($IgD^{-}CD38^{+}CD73^{+}CD80^{+}$) B-cells (Fig. 3). GC B-cells were the only population to stain brightly with GL7 (Fig. 3A). Unlike human naive and memory B-cells, the KN343 antibody did not show significant binding to any of the populations in mice (Fig. 3B). Staining with murine CD22-Fc showed the opposite staining pattern of GL7, with naive and memory B-cells staining brightly (Fig. 3C). A polyclonal linkage-independent anti-Neu5Gc antibody (5) exhibited the same pattern as mCD22-Fc (Fig. 3D). Although CD22 expression remained high on all three populations (Fig. 3E), liposomal nanoparticles

displaying murine CD22 ligand ^{BP}A_{NeuGc} showed enhanced recognition by GC B-cells (Fig. 3F). These results demonstrate that unmasking of CD22 on GC B-cells relative to naive and memory B-cells is conserved between the mouse and human.

Direct Detection of Sulfated Glycans on Human B-cells by Mass Spectrometry—Given what is known about the specificity of the KN343 antibody, the staining of naive human B-cells with KN343 has implied the presence of sulfated sialosides (15). To obtain direct experimental evidence for sulfated sialosides on human B-cells, 200×10^6 tonsillar B-cells were purified by negative selection for matrix-assisted laser desorption ionization-mass spectrometry (MALDI-MS)-based sulfoglycomic analysis, focusing specifically on selective detection of the fractionated and hence enriched permethylated sulfated glycans in negative ion mode. From human tonsillar B-cells, sulfated complex type *N*-glycans were readily detected (Fig. 4A), which were largely resistant to digestion with a sialidase specific for α 2,3-sialosides (Fig. 4B). These data confirm that α 2–6-linked Neu5Ac sialosides bearing a sulfate modification are abundant on human B-cells. Analysis of *O*-glycans derived from these samples also revealed the presence of sulfated glycans (Fig. 4C). In a separate experiment, B-cells were purified from the peripheral blood of a healthy donor. Cells were activated by BCR stimulation along with co-stimulation through TLR9. Activated cells proliferated, as evident by dilution of CFSE, yet retained KN343 staining (Fig. 4D). Sulfoglycomic profiling of these activated B-cells confirmed the presence of sulfated and sialylated complex *N*-glycans (Fig. 4E) that were resistant to digestion with a α 2,3-sialidase (Fig. 4F). *O*-Glycans released from these samples also revealed the presence of sulfated α 2–6-linked sialosides (Fig. 4, G and H). Similar MALDI-MS analyses were carried out on glycans derived from murine B-cells, but no significant signal attributable to sulfated glycan was detected to support its presence at any appreciable amount, despite a good recovery and detection of the non-sulfated glycans. Thus, the MS-based sulfoglycomic profiling reveals that sulfated sialylated glycans are readily detected on primary human B-cells and are not lost 3 days after *in vitro* B-cell activation, but similar sulfated glycans are not present or not detected on murine B-cells.

Glycan Binding Specificity of GL7 and KN343—As described above, and as shown previously (6, 15), the antibodies GL7 and KN343 are valuable tools for detecting GC B-cell-specific glycosylation patterns in mice and humans, respectively. Earlier studies probing the glycan specificity of GL7 and KN343 using a small and select panel of sialosides revealed that GL7 prefers Neu5Ac α 2–6-linked to an underlying LacNAc (6), whereas KN343 recognizes Neu5Ac α 2–6-linked to an underlying LacNAc bearing a sulfate group on the 6'-position of the GlcNAc (15). To investigate the specificities of these antibodies in greater detail, we used a glycan microarray to assess the specificity of each antibody toward a large number of glycans. Glycan microarrays provide a semi-quantitative and comparative analysis for the binding of glycan-binding proteins to glycans covalently printed onto a glass slide (26). Accordingly, we used a sialoside array consisting of 57 sialosides, along with 2 non-sialylated glycans as controls, containing a variety of Neu5Ac- or Neu5Gc-containing glycans, which are α 2–6- or α 2–3-

linked to an underlying LacNAc on a linear, *N*-, or *O*-linked scaffold (Fig. 5) (22).

KN343 binding to the sialoside array was highly specific, as it recognized only two glycans (Fig. 6A). The glycans recognized by KN343 were Neu5Ac α 2–6Gal β 1–4(6-sulfo)GlcNAc and Neu5Gc α 2–6Gal β 1–4(6-sulfo)GlcNAc, which is in keeping with the specificity of this antibody for glycans bearing an α 2–6-linked Sia residue on a sulfated LacNAc core (15). It is noteworthy that the ability of KN343 to recognize the Neu5Gc-containing sulfated glycan was not reported previously. To be certain that KN343 recognizes Neu5Gc α 2–6Gal β 1–4(6-sulfo)GlcNAc with an avidity in the same range of the corresponding Neu5Ac glycan, the two glycans were printed in 2-fold serial dilutions (Fig. 6B). At lower printing concentrations, a minor preference for the Neu5Ac-containing glycan was evident, but was not enhanced, demonstrating that the Neu5Gc-sulfated glycan is a good ligand for KN343. The fact that Neu5Gc is abundant on murine B-cells (Fig. 3D), yet is not stained by KN343 (Fig. 3B), reinforces our mass spectrometry results indicating that sulfated CD22 ligands are not present at detectable amounts on murine B-cells.

The antibody GL7 showed remarkable specificity for α 2–6-linked Neu5Ac on the sialoside microarray (Fig. 6C). Indeed, no glycans that contained α 2,3-linked sialosides or NeuGc-containing sialoside showed appreciable recognition by GL7. Within the family of α 2–6-linked Neu5Ac structures, GL7 displayed an unexpected preference for structures with extended di- and tri-LacNAc repeats on either *O*- and *N*-glycans. This specificity was evident on four individual sets of glycans as follows: core 2 *O*-glycans (glycans 44–45); core 3 *O*-glycans (glycans 46–47); core 4 *O*-glycans (glycans 48–49), and biantennary *N*-glycans (glycans 53–55). Linear structures (glycans 38–40) also displayed this trend, but the effect was not as pronounced, suggesting that underlying structural determinants on *O*- and *N*-glycans preclude binding when the α 2–6-linked Neu5Ac is presented on only a single LacNAc unit. This trend is not observed for the α 2–6-specific SNA (Fig. 6D), confirming that the results obtained with GL7 do not simply reflect differential printing efficiency or presentation of the extended glycans. The requirement for multi-LacNAc units to confer binding of sialosides by GL7 was validated in solution using an ELISA, where immobilized GL7 was probed with glycans containing a biotin tag at their reducing end. Using a disialylated biantennary *N*-glycan bearing either one or three LacNAc repeats on each arm, it was readily evident that the extended sialoside had an \sim 100-fold decrease in IC₅₀ for GL7 (Fig. 6E).

To test whether increased binding of GL7 to sialosides with extended poly-LacNAc units relates to the ability of GL7 to strongly stain murine GC B-cells, naive and GC B-cells were probed with the LEL because it is specific for LacNAc units and can be used to quantitatively assess the number of LacNAc units on a cell surface (27). We found that murine GC B-cells had higher staining with LEL compared with naive B-cells (Fig. 6F). Thus, GL7 displays a previously unrecognized preference for α 2–6-linked Neu5Ac sialosides extended with more than one LacNAc repeat, and enrichment of these structures on murine GC B-cells may contribute to the bright staining that GL7 displays toward murine GC B-cells.

Unmasking of CD22 in the Germinal Center

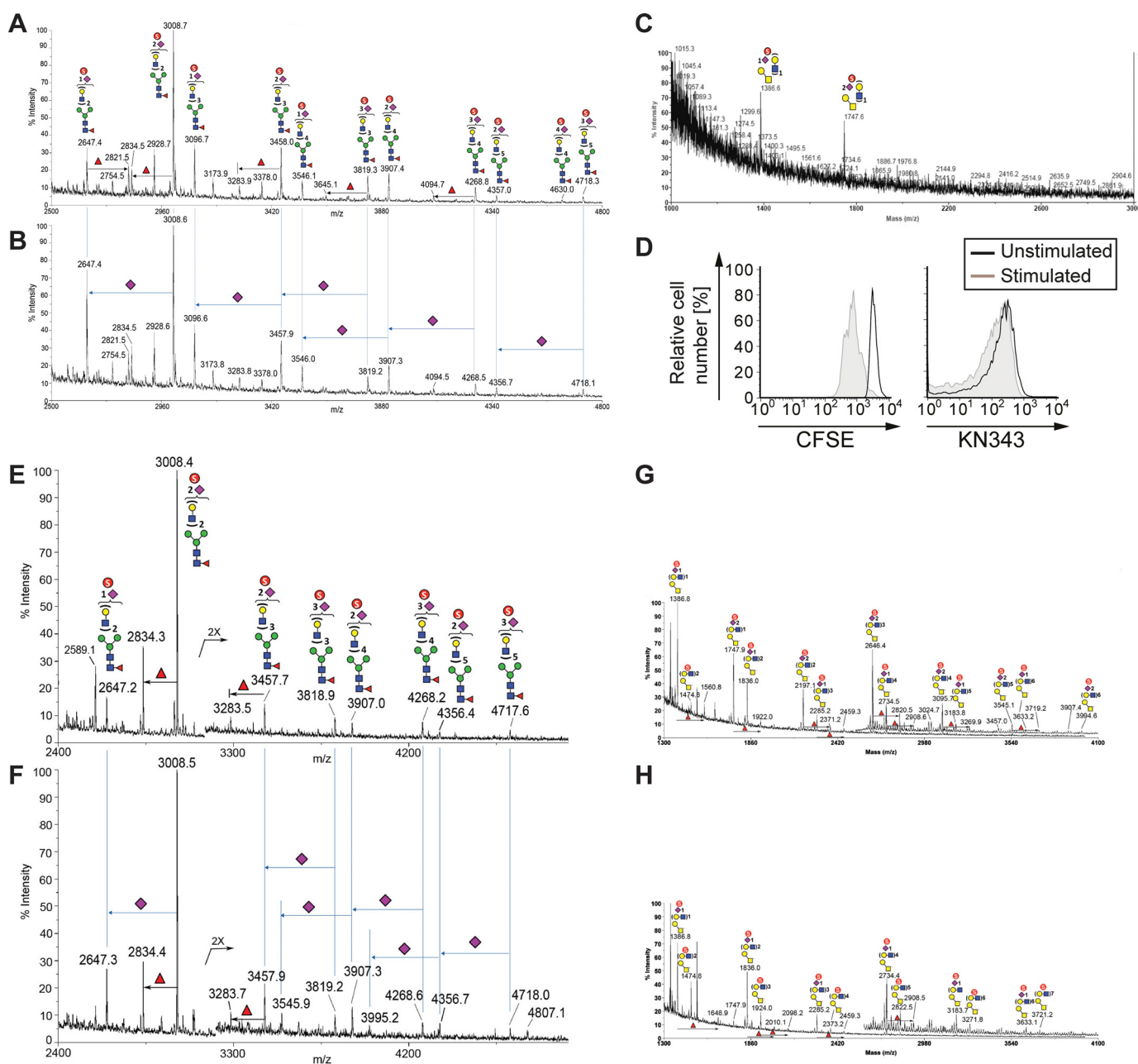


FIGURE 4. Mass spectrometry analyses reveal that human tonsillar B-cells contain an abundance of sulfated sialylated glycans. A–C, human tonsillar B-cells (200×10^6) were purified by negative selection, and N-glycans from extracted glycoproteins were released by peptide:N-glycosidase F digestion, without (A) or with (B) further digestion by an α 2-3-specific sialidase and permethylated, and the enriched sulfated glycan fractions were analyzed by MALDI-MS in negative ion mode. C, analysis of O-glycan analysis of human tonsillar B-cells. D, human peripheral blood B-cells were purified by negative selection, labeled with CFSE, and stimulated with a combination of anti-IgM, anti-IgG, anti-IgA, and CpG2006. After 3 days in culture, stimulated cells were compared with non-stimulated cells for levels of CFSE and KN343 staining. E–H, similar negative ion mode sulfoglycomic profilings were carried out on permethylated N-glycans (E and F) and from stimulated peripheral blood B-cells (G and H) before (E and G) and after (F and H) digestion with a α 2-3-specific sialidase. The major [M - H]⁻ sulfated N-glycan and O-glycan signals were assigned by glycosyl compositions fitted in terms of Hex, HexNAc, fucose, and NeuAc, and the most likely structures annotated using the standard schematic symbols recommended by the Consortium for Functional Glycomics, without implying specific linkages and stereochemistry. Structures related by a single NeuAc residue difference are indicated in the mass spectra for sialidase-treated sample.

Biochemical Analysis of mCD22 and hCD22 Glycan Binding Specificity—To more precisely understand how the specificity of human and murine CD22 relates to the relevant sialosides on naive and GC B-cells, four glycans were chemo-enzymatically synthesized (Fig. 7A). This small panel of glycans consisted of the following: Neu5Ac α 2-6Gal β 1-4-GlcNAc, Neu5Ac α 2-6Gal β 1-4(6-sulfo)GlcNAc, Neu5Gc α 2-6Gal β 1-4-GlcNAc, and Neu5Gc α 2-6Gal β 1-4(6-sulfo)GlcNAc. Com-

petitive bead binding assays were carried out in conjunction with flow cytometry to analyze binding of these glycans to human CD22 and murine CD22 (Fig. 7B). For human CD22, the sulfate group afforded a clear 2-fold decrease in the IC₅₀ value for either the Neu5Ac- or Neu5Gc-bearing glycan. Consistent with previous findings, minimal discrimination was observed between the Neu5Ac- and the Neu5Gc-bearing glycans for human CD22, which is in contrast to murine CD22 that had a

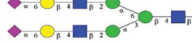
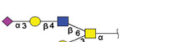
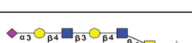
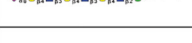
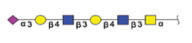
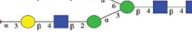
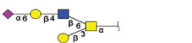
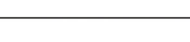
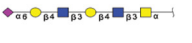
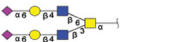
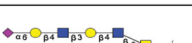
Chart#	Structure	Chart#	Structure	Chart#	Structure	Chart#	Structure
1		18		36		53	
2		19		37		54	
3		20		38		55	
4		21		39		56	
5		22		40		57	
6		23		41		58	
7		24		42		59	
8		25		43			
9		26		44			
10		27		45			
11		28		46			
12		29		47			
13		30		48			
14		31		49			
15		32		50			
16		33		51			
17		34		52			
		35					

FIGURE 5. List of glycans on the sialoside array. Compounds numbered in blue are α 2–3-linked sialosides, whereas compounds numbered in red are α 2–6-linked sialosides, and structures of the individual glycans are shown, where purple diamonds are *N*-acetylneuraminic acid (Neu5Ac), light blue diamonds are *N*-glycolylneuraminic acid (Neu5Gc), yellow circles are galactose (Gal), blue squares are *N*-acetylglucosamine (GlcNAc), yellow squares are *N*-acetylgalactosamine (GalNAc), and green circles are mannose (Man).

20-fold lower IC_{50} value for Neu5Gc α 2–6Gal β 1–4-GlcNAc compared with its Neu5Ac counterpart. Unexpectedly, the sulfate group provided a 10- and 4-fold decrease in IC_{50} for mCD22 binding to the Neu5Ac- and Neu5Gc-bearing glycans, respectively.

As an independent measure of specificity, the Fc-chimeras of human and murine CD22 were applied to the sialoside microarray (Fig. 8A). As expected, both proteins showed remarkable specificity for α 2–6-linked sialosides. Consistent with the bead binding assay, as well as previous glycan array data (17), the top

Unmasking of CD22 in the Germinal Center

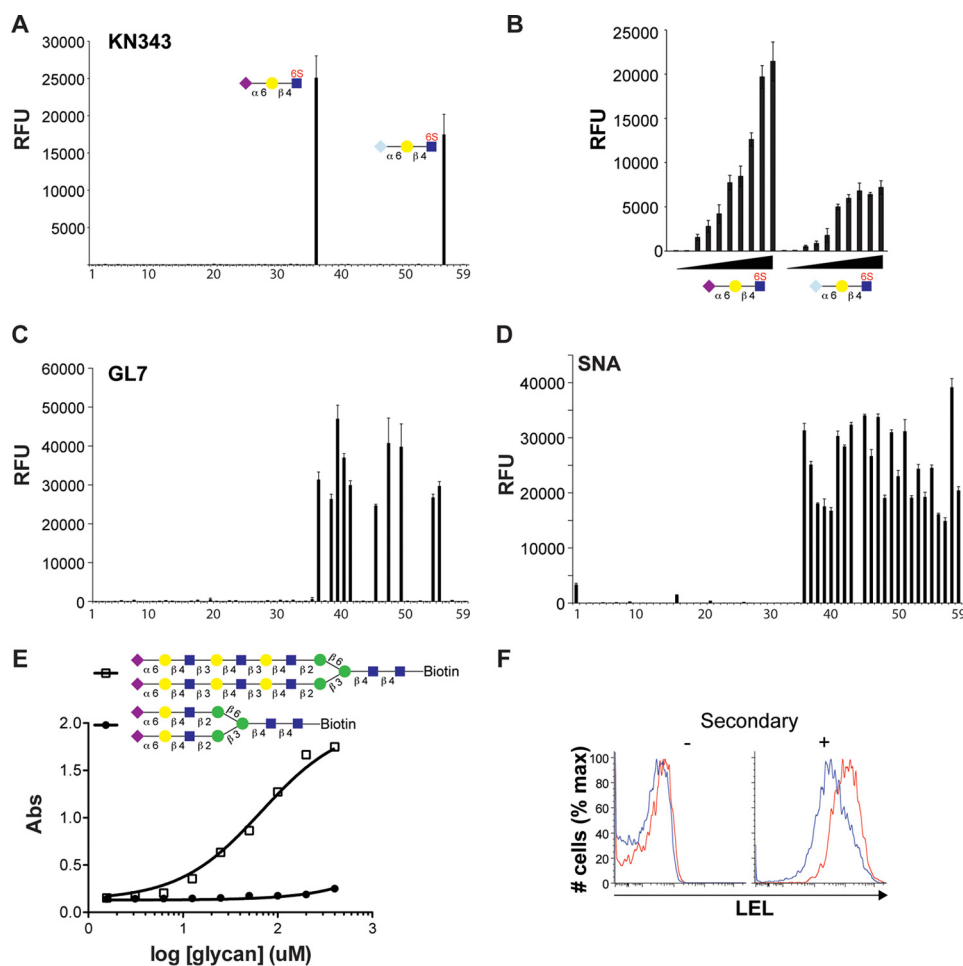


FIGURE 6. Glycan binding specificity of the KN343 and GL7 antibodies. *A*, probing the 59 glycan sialoside microarray with KN343 demonstrates that it selectively recognizes Neu5Ac α 2-6Gal β 1-4(6S)GlcNAc and Neu5Gc α 2-6Gal β 1-4(6S)GlcNAc. *B*, printing concentration of Neu5Ac α 2-6Gal β 1-4(6S)GlcNAc and Neu5Gc α 2-6Gal β 1-4(6S)GlcNAc was titrated in 2-fold serial dilutions and probed with KN343. *C* and *D*, probing a 59 glycan sialoside microarray with GL7 (*C*) and SNA (*D*) demonstrates that GL7 selectively recognizes glycans containing terminal α 2-6-linked Neu5Ac and prefers structures containing more than one LacNAc repeat. A complete list of glycans is described in Fig. 5. *E*, direct binding of a complex *N*-glycan containing 1 (closed circles) or 3 (open squares) LacNAc units per arm to GL7 by ELISA. *F*, staining of naive (CD19⁺CD95⁻CD38⁺GL7⁻; blue) and GC (CD19⁺CD95⁺CD38⁻GL7⁺; red) B-cells for LEL. The histogram on the left represents background staining without secondary antibody. RFU, relative fluorescence units.

hit for hCD22 was Neu5Ac α 2-6Gal β 1-4(6-sulfo)GlcNAc (Fig. 8B). There was no clear preference for specific *N*- or *O*-glycans nor was there a preference for extended poly-LacNAc structures as observed with GL7 (Fig. 6C). For murine CD22, Neu5Gc was clearly preferred over Neu5Ac sialosides, with the exception of Neu5Ac α 2-6Gal β 1-4(6-sulfo)GlcNAc (Fig. 8B); this result is consistent with the bead binding assay. Overall, the more qualitative glycan microarray results support the solution studies, which demonstrate that human CD22 has a clear preference for sulfated glycans, whereas murine CD22 has a preference for NeuGc. These preferences match the glycans found on naive and memory B-cells from mice and humans. These data demonstrate the presence of high affinity CD22 ligands on naive and memory B-cells maintain CD22 in a masked state, whereas GC B-cells from both mice and humans lose the preferred sialoside ligand for CD22, resulting in unmasking of CD22 relative to naive and memory B-cells (Fig. 9).

Discussion

Antibody affinity maturation within the GC is a critical aspect of immunity that takes place through a program involv-

ing mutation-driven BCR diversification, selection of clones with the highest affinity, and expansion of selected clones (14). Expression patterns unique to GC B-cells are of great interest for providing a deeper understanding of the GC reaction. Accordingly, the unexplored functional significance of distinct patterns of glycosylation on GC B-cells has the potential to yield critical insights into the GC reaction. Indeed, two changes in glycosylation on GC B-cells, detected by the lectin peanut agglutinin and the antibody GL7, are widely used to identify the GC, yet the functional significance of these changes in glycosylation is unknown. We have shown that the loss of the preferred CD22 ligand on GC B-cells is a conserved feature in both mice and humans, but it occurs through different biochemical mechanisms unique to the nuances of the preferred ligand of CD22 in these two species. The result in both species is the unmasking of CD22 on GC B-cells, relative to naive and memory B-cells, which manifests as an enhanced ability of GC B-cells to interact with *trans* ligands.

On GC B-cells from mice and humans, lower levels of *cis* ligands were clearly evident by flow cytometry. This finding had been previously shown in mice (6) but not directly in humans

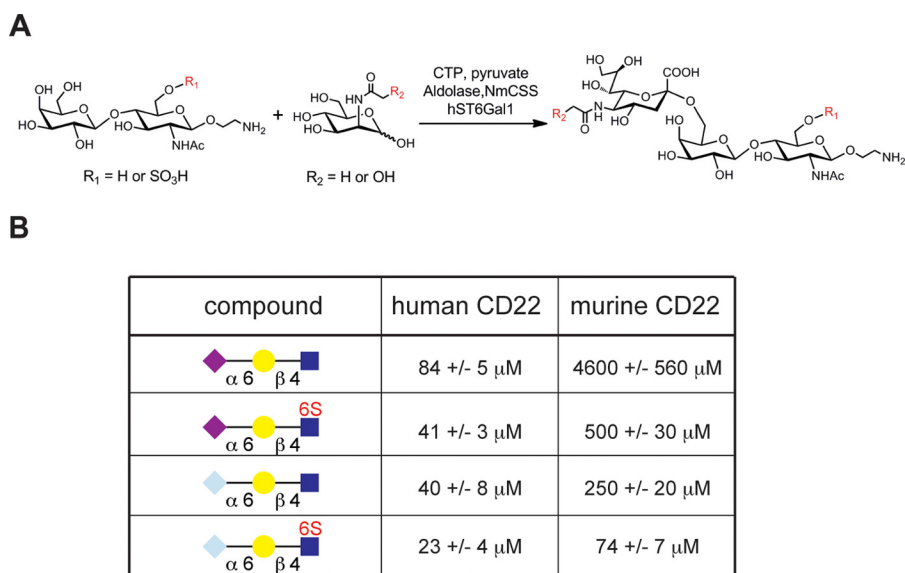


FIGURE 7. **IC₅₀ values for recognition of a small panel of sialosides by human and murine CD22.** *A*, scheme for the chemoenzymatic synthesis of four representative glycans used for probing the ligand specificity of human and murine CD22. LacNAc or its 6-*O*-sulfate-modified derivative was coupled to either Neu5Ac or Neu5Gc in an α 2–6-linked glycosidic linkage using the human ST6Gal1 enzyme. The source of Neu5Ac and Neu5Gc was from ManNAc and *N*-glycolylmannosamine, respectively, using the aldolase *N. meningitidis* sialic acid synthetase (NmCSS) in a coupled reaction with the sialyltransferase ST6Gal1. *B*, binding affinity of the four chemo-enzymatically synthesized trisaccharides was determined by a competitive bead binding assay with human and murine CD22. Values represent the mean and standard deviations for four independent experiments.

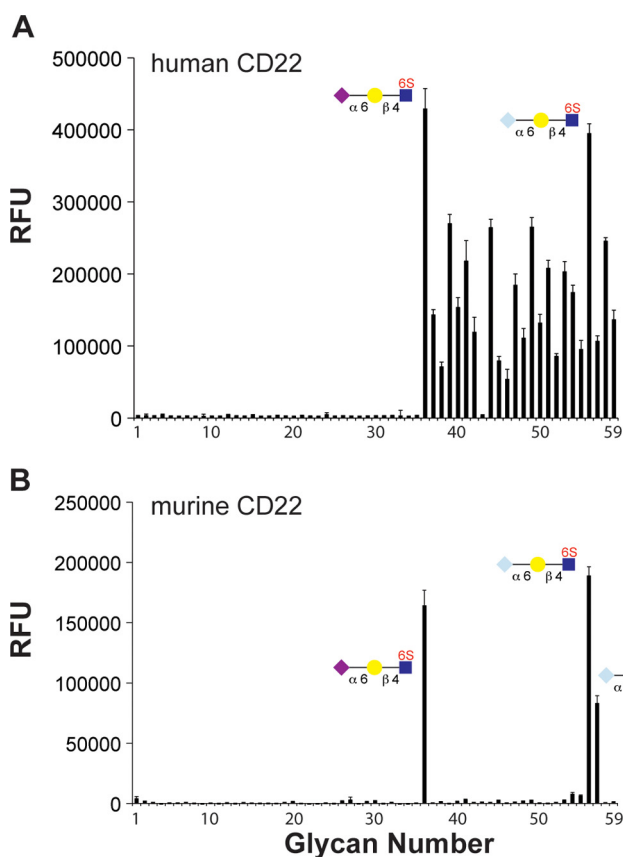


FIGURE 8. **Analysis of glycan binding specificity of human and murine CD22 by glycan microarray.** *A* and *B*, probing the 59 glycan sialoside microarray with human CD22-Fc (*A*) and murine CD22-Fc (*B*). Selected glycans are shown, and a complete list of glycans is described in Fig. 5. RFU, relative fluorescence units.

using the appropriate markers to distinguish GC B-cells (28). In humans, loss of the high affinity human CD22 ligand occurs through loss of α 2–6-linked sialosides bearing a 6-*O*-sulfate

modification on GlcNAc residues. Validating a proposal made previously (15), the KN343 antibody showed remarkable specificity for α 2–6-linked sialosides bearing the sulfate modification and that this sulfate modification is readily detected on primary human B-cells by MS sulfoglycomic analysis. As glycans bearing this sulfate modification were clearly shown to be the highest affinity ligands for human CD22 in both solution binding studies and a glycan microarray, these results provide concrete evidence that loss of sulfated glycans on human GC B-cells results in lower levels of *cis* ligands for CD22, leading to its unmasking relative to naive and memory B-cells.

Multiple lines of evidence enable us to provide the first evidence that this sulfate modification is absent on murine B-cells. We show that KN343 recognizes Neu5Gc α 2–6Gal β 1–4(6-sulfo)GlcNAc and its Neu5Ac counterpart as ligands, yet KN343 fails to stain naive murine B-cells. Coupled with the inability to detect sulfated glycans on murine B-cells by MS sulfoglycomic analysis, we conclude that sulfated CD22 ligands are found on human B-cells and not murine B-cells. Instead of changes in the sulfate modification, loss of the high affinity CD22 ligands on murine GC B-cells stems from loss of Neu5Gc (6). Comparing the affinity gain provided by the sulfate modification for human CD22 (2-fold) to the affinity gain afforded by the change from Neu5Ac to Neu5Gc (20-fold) suggests that additional factors could also be at play on human GC B-cells that contribute to unmasking of CD22. One possibility is differential levels of 9-*O*-acetylation of sialic acid because it is known to prevent recognition by CD22 (29, 30).

In both mice and humans, high affinity CD22 ligands returns on memory B-cells. Post-GC B-cells (memory B-cells) clearly regained the high affinity CD22 ligand, and pre-GC (*in vitro* stimulated) human B-cells also expressed the high affinity CD22 ligand, as we demonstrated here for human B-cells and demonstrated previously for mouse B-cells (31). The results

Unmasking of CD22 in the Germinal Center

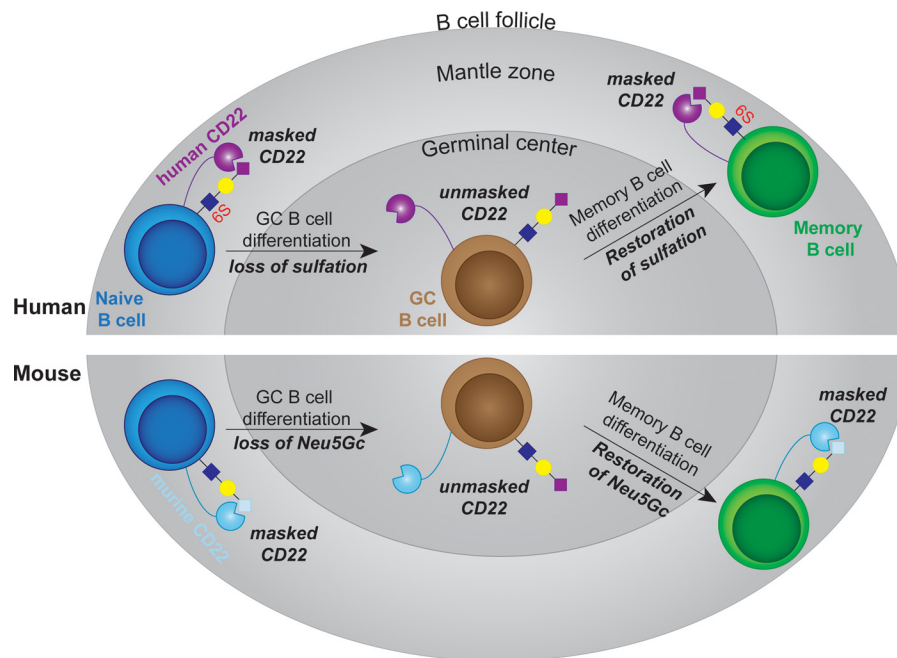


FIGURE 9. Model for the conserved nature of unmasking of CD22 in the GC of mice and humans. *Top*, in human, CD22 on naive B-cells in mantle zone is masked through interactions with its high affinity ligand (Neu5Ac α 2-6Gal β 1-4(6S)GlcNAc). Loss of the sulfate modification on GC B-cells results in the appearance of Neu5Ac α 2-6Gal β 1-4GlcNAc glycans, which have a lower affinity for human CD22. The lower affinity *cis* ligands on GC B-cells will place CD22 in an unbound state (unmasked) at a higher frequency, enabling it to interact better with *trans* ligands. This sulfate modification is restored on memory B-cells, returning CD22 to a masked state. *Bottom*, in mice, naive B-cells have abundant levels of Neu5Gc α 2-6Gal β 1-4GlcNAc, the preferred ligand of murine CD22, maintaining CD22 in a masked state. Loss of Neu5Gc on GC B-cells results in the appearance of glycans terminating in Neu5Ac α 2-6Gal β 1-4GlcNAc, which unmask CD22 due to the lower binding affinity of murine CD22 for the NeuAc-containing glycan. Paralleling the results in humans, the high affinity ligand of murine CD22 is restored on memory B-cells, returning CD22 to a masked state.

demonstrate that loss of the high affinity CD22 ligand and unmasking of CD22 on GC B-cells is a transient phenomenon unique to the GC.

The conserved loss of high affinity ligands on GC B-cells in mice and humans resulting in unmasking of CD22 suggests an associated function. Decreased levels of *cis* ligands and subsequent unmasking of CD22 on GC B-cells has the potential to participate in the biology of the GC B-cells in numerous ways. Recently, we have shown that *trans* ligands on cells expressing a cell surface autoantigen recruit CD22 to the immunological synapse (7). Therefore, one intriguing possibility is that B-cells acquiring autoreactivity in GC to cell surface autoantigens may be clonally deleted through enhanced sensitivity of CD22 *trans* ligand interactions. Recently, B-cell homing to the gut was shown to occur through CD22-mediated interactions with *trans* ligand interactions expressed on specialized endothelial cells (9). As coordinated movement of GC B-cells between the light zone and dark zone of the GC is critical in the selection process (14), CD22 could participate in this migration. Another possibility where unmasking of CD22 on GC B-cells could make an impact is in B-T cell interactions (32). Indeed, several studies have suggested that CD22 can modulate B-T cell interactions (12, 32–35). Decreased *cis* ligands on GC B-cells could also be a means of modulating the interactions between CD22 and the BCR to regulate B-cell signaling or endocytosis. Studies are underway to examine how CD22 ligands impact the GC reaction as a whole.

In summary, loss of the high affinity ligand on GC B-cells occurs in mice and humans through different mechanisms. This loss results in unmasking of CD22 on GC B-cells relative to

naive and is transient because memory B-cells return CD22 ligands to the state found on naive B-cells. The fact that different mechanisms have evolved in mice and humans to unmask CD22 on GC B-cells strongly suggests an important role for CD22-ligand interactions in the GC reaction.

Author Contributions—M. S. M., N. K., and J. C. P. conceived and coordinated the study and wrote the paper. W. P. and Y. H. performed the experiments described in Fig. 6. S. W. and K. K. acquired and interpreted mass spectrometry data shown in Fig. 4. B. M. A. provided technical assistance. R. M. acquired and interpreted glycan array experiments shown in Figs. 6 and 8. R. K. provided KN343 antibody and helped interpret data acquired with this antibody. All authors analyzed the results and approved the final version of the manuscript.

Acknowledgments—We thank Professor Anne Feeney for coordinating the receipt of human tonsils through the Scripps Green hospital. The MS data were acquired at the Core Facilities for Protein Structural Analysis at Academia Sinica, supported under the Taiwan National Core Facility Program for Biotechnology, NSC Grants 101-2319-B-001-003 and 102-2319-B-001-003.

References

1. Macauley, M. S., Crocker, P. R., and Paulson, J. C. (2014) Siglec-mediated regulation of immune cell function in disease. *Nat. Rev. Immunol.* **14**, 653–666
2. Nitschke, L. (2014) CD22 and Siglec-G regulate inhibition of B-cell signaling by sialic acid ligand binding and control B-cell tolerance. *Glycobiology* **24**, 807–817
3. Crocker, P. R., Paulson, J. C., and Varki, A. (2007) Siglecs and their roles in

- the immune system. *Nat. Rev. Immunol.* **7**, 255–266
4. Müller, J., Obermeier, I., Wöhner, M., Brandl, C., Mrotzek, S., Angermüller, S., Maity, P. C., Reth, M., and Nitschke, L. (2013) CD22 ligand-binding and signaling domains reciprocally regulate B-cell Ca²⁺ signaling. *Proc. Natl. Acad. Sci. U.S.A.* **110**, 12402–12407
 5. Cariappa, A., Takematsu, H., Liu, H., Diaz, S., Haider, K., Boboila, C., Kallou, G., Connole, M., Shi, H. N., Varki, N., Varki, A., and Pillai, S. (2009) B cell antigen receptor signal strength and peripheral B cell development are regulated by a 9-*O*-acetyl sialic acid esterase. *J. Exp. Med.* **206**, 125–138
 6. Naito, Y., Takematsu, H., Koyama, S., Miyake, S., Yamamoto, H., Fujinawa, R., Sugai, M., Okuno, Y., Tsujimoto, G., Yamaji, T., Hashimoto, Y., Itohara, S., Kawasaki, T., Suzuki, A., and Kozutsumi, Y. (2007) Germinal center marker GL7 probes activation-dependent repression of *N*-glycolylneuraminic acid, a sialic acid species involved in the negative modulation of B-cell activation. *Mol. Cell. Biol.* **27**, 3008–3022
 7. Macauley, M. S., and Paulson, J. C. (2014) Siglecs induce tolerance to cell surface antigens by BIM-dependent deletion of the antigen-reactive B cells. *J. Immunol.* **193**, 4312–4321
 8. Macauley, M. S., Pfrenge, F., Rademacher, C., Nycholat, C. M., Gale, A. J., von Drygalski, A., and Paulson, J. C. (2013) Antigenic liposomes displaying CD22 ligands induce antigen-specific B cell apoptosis. *J. Clin. Invest.* **123**, 3074–3083
 9. Lee, M., Kiefel, H., LaJevic, M. D., Macauley, M. S., Kawashima, H., O'Hara, E., Pan, J., Paulson, J. C., and Butcher, E. C. (2014) Transcriptional programs of lymphoid tissue capillary and high endothelium reveal control mechanisms for lymphocyte homing. *Nat. Immunol.* **15**, 982–995
 10. Nitschke, L., Floyd, H., Ferguson, D. J., and Crocker, P. R. (1999) Identification of CD22 ligands on bone marrow sinusoidal endothelium implicated in CD22-dependent homing of recirculating B cells. *J. Exp. Med.* **189**, 1513–1518
 11. Razi, N., and Varki, A. (1998) Masking and unmasking of the sialic acid-binding lectin activity of CD22 (Siglec-2) on B lymphocytes. *Proc. Natl. Acad. Sci. U.S.A.* **95**, 7469–7474
 12. Collins, B. E., Blixt, O., DeSieno, A. R., Bovin, N., Marth, J. D., and Paulson, J. C. (2004) Masking of CD22 by cis ligands does not prevent redistribution of CD22 to sites of cell contact. *Proc. Natl. Acad. Sci. U.S.A.* **101**, 6104–6109
 13. Collins, B. E., Blixt, O., Han, S., Duong, B., Li, H., Nathan, J. K., Bovin, N., and Paulson, J. C. (2006) High affinity ligand probes of CD22 overcome the threshold set by cis ligands to allow for binding, endocytosis, and killing of B cells. *J. Immunol.* **177**, 2994–3003
 14. Victoria, G. D., and Nussenzweig, M. C. (2012) Germinal centers. *Annu. Rev. Immunol.* **30**, 429–457
 15. Kimura, N., Ohmori, K., Miyazaki, K., Izawa, M., Matsuzaki, Y., Yasuda, Y., Takematsu, H., Kozutsumi, Y., Moriyama, A., and Kannagi, R. (2007) Human B-lymphocytes express α 2-6-sialylated 6-sulfo-*N*-acetylglucosamine serving as a preferred ligand for CD22/Siglec-2. *J. Biol. Chem.* **282**, 32200–32207
 16. Chou, H. H., Takematsu, H., Diaz, S., Iber, J., Nickerson, E., Wright, K. L., Muchmore, E. A., Nelson, D. L., Warren, S. T., and Varki, A. (1998) A mutation in human CMP-sialic acid hydroxylase occurred after the Homo-Pan divergence. *Proc. Natl. Acad. Sci. U.S.A.* **95**, 11751–11756
 17. Blixt, O., Head, S., Mondala, T., Scanlan, C., Huflejt, M. E., Alvarez, R., Bryan, M. C., Fazio, F., Calarese, D., Stevens, J., Razi, N., Stevens, D. J., Skehel, J. J., van Die, I., Burton, D. R., et al. (2004) Printed covalent glycan array for ligand profiling of diverse glycan binding proteins. *Proc. Natl. Acad. Sci. U.S.A.* **101**, 17033–17038
 18. Kelm, S., Schauer, R., Manuguerra, J. C., Gross, H. J., and Crocker, P. R. (1994) Modifications of cell surface sialic acids modulate cell adhesion mediated by sialoadhesin and CD22. *Glycoconj. J.* **11**, 576–585
 19. Sakuma, K., Chen, G. Y., Aoki, M., and Kannagi, R. (2012) Induction of 6-sulfated glycans with cell adhesion activity via T-bet and GATA-3 in human helper T cells. *Biochim. Biophys. Acta* **1820**, 841–848
 20. Wang, S. H., Tsai, C. M., Lin, K. L., and Khoo, K. H. (2013) Advanced mass spectrometry and chemical analyses reveal the presence of terminal disialyl motif on mouse B-cell glycoproteins. *Glycobiology* **23**, 677–689
 21. Khoo, K. H., and Yu, S. Y. (2010) Mass spectrometric analysis of sulfated *N*- and *O*-glycans. *Methods Enzymol.* **478**, 3–26
 22. Nycholat, C. M., McBride, R., Ekiert, D. C., Xu, R., Rangarajan, J., Peng, W., Razi, N., Gilbert, M., Wakarchuk, W., Wilson, I. A., and Paulson, J. C. (2012) Recognition of sialylated poly-*N*-acetylglucosamine chains on *N*- and *O*-linked glycans by human and avian influenza A virus hemagglutinins. *Angew. Chem. Int. Ed. Engl.* **51**, 4860–4863
 23. Blixt, O., Collins, B. E., van den Nieuwenhof, I. M., Crocker, P. R., and Paulson, J. C. (2003) Sialoside specificity of the Siglec family assessed using novel multivalent probes: identification of potent inhibitors of myelin-associated glycoprotein. *J. Biol. Chem.* **278**, 31007–31019
 24. Rillahan, C. D., Macauley, M. S., Schwartz, E., He, Y., McBride, R., Arlian, B. M., Rangarajan, J., Fokin, V. V., and Paulson, J. C. (2014) Disubstituted sialic acid ligands targeting siglecs CD33 and CD22 associated with myeloid leukaemias and B cell lymphomas. *Chem. Sci.* **5**, 2398–2406
 25. Duong, B. H., Tian, H., Ota, T., Completo, G., Han, S., Vela, J. L., Ota, M., Kubitz, M., Bovin, N., Paulson, J. C., Paulson, J., and Nemazee, D. (2010) Decoration of T-independent antigen with ligands for CD22 and Siglec-G can suppress immunity and induce B cell tolerance *in vivo*. *J. Exp. Med.* **207**, 173–187
 26. Rillahan, C. D., and Paulson, J. C. (2011) Glycan microarrays for decoding the glycome. *Annu. Rev. Biochem.* **80**, 797–823
 27. Croci, D. O., Cerliani, J. P., Dalotto-Moreno, T., Méndez-Huergo, S. P., Mascanfroni, I. D., Dergan-Dylon, S., Toscano, M. A., Caramelo, J. J., García-Vallejo, J. J., Ouyang, J., Mesri, E. A., Junttila, M. R., Bais, C., Shipp, M. A., Salatino, M., and Rabinovich, G. A. (2014) Glycosylation-dependent lectin-receptor interactions preserve angiogenesis in anti-VEGF refractory tumors. *Cell* **156**, 744–758
 28. Kannagi, R., Ohmori, K., and Kimura, N. (2009) Anti-oligosaccharide antibodies as tools for studying sulfated sialoglycoconjugate ligands for siglecs and selectins. *Glycoconj. J.* **26**, 923–928
 29. Sjöberg, E. R., Powell, L. D., Klein, A., and Varki, A. (1994) Natural ligands of the B-cell adhesion molecule Cd22- β can be masked by 9-*O*-acetylation of sialic acids. *J. Cell Biol.* **126**, 549–562
 30. Pillai, S., Netravali, I. A., Cariappa, A., and Mattoo, H. (2012) Siglecs and immune regulation. *Annu. Rev. Immunol.* **30**, 357–392
 31. Comelli, E. M., Sutton-Smith, M., Yan, Q., Amado, M., Panico, M., Gilmartin, T., Whisenant, T., Lanigan, C. M., Head, S. R., Goldberg, D., Morris, H. R., Dell, A., and Paulson, J. C. (2006) Activation of murine CD4⁺ and CD8⁺ T lymphocytes leads to dramatic remodeling of *N*-linked glycans. *J. Immunol.* **177**, 2431–2440
 32. Naito-Matsui, Y., Takada, S., Kano, Y., Iyoda, T., Sugai, M., Shimizu, A., Inaba, K., Nitschke, L., Tsubata, T., Oka, S., Kozutsumi, Y., and Takematsu, H. (2014) Functional evaluation of activation-dependent alterations in the sialoglycan composition of T cells. *J. Biol. Chem.* **289**, 1564–1579
 33. Aruffo, A., Kanner, S. B., Sgroi, D., Ledbetter, J. A., and Stamenkovic, I. (1992) CD22-mediated stimulation of T cells regulates T-cell receptor/CD3-induced signaling. *Proc. Natl. Acad. Sci. U.S.A.* **89**, 10242–10246
 34. Fujimoto, M., Kuwano, Y., Watanabe, R., Asashima, N., Nakashima, H., Yoshitake, S., Okochi, H., Tamaki, K., Poe, J. C., Tedder, T. F., and Sato, S. (2006) B cell antigen receptor and CD40 differentially regulate CD22 tyrosine phosphorylation. *J. Immunol.* **176**, 873–879
 35. Yuan, J., Yu, M., Cao, A. L., Chen, X., Zhang, L. H., Song, Y., Cheng, X., Zhou, Z. H., Wang, M., Guo, H. P., Du, R., and Liao, Y. H. (2013) A novel epitope from CD22 regulates Th1 and Th17 cell function in systemic lupus erythematosus. *PLoS ONE* **8**, e64572

**Unmasking of CD22 Co-receptor on Germinal Center B-cells Occurs by
Alternative Mechanisms in Mouse and Man**

Matthew S. Macauley, Norihito Kawasaki, Wenjie Peng, Shui-Hua Wang, Yuan He,
Britni M. Arlian, Ryan McBride, Reiji Kannagi, Kay-Hooi Khoo and James C. Paulson

J. Biol. Chem. 2015, 290:30066-30077.

doi: 10.1074/jbc.M115.691337 originally published online October 27, 2015

Access the most updated version of this article at doi: [10.1074/jbc.M115.691337](https://doi.org/10.1074/jbc.M115.691337)

Alerts:

- [When this article is cited](#)
- [When a correction for this article is posted](#)

[Click here](#) to choose from all of JBC's e-mail alerts

This article cites 35 references, 18 of which can be accessed free at
<http://www.jbc.org/content/290/50/30066.full.html#ref-list-1>